

# Theory and simulation of photogeneration and transport in Si-SiO<sub>x</sub> superlattice absorbers

U. Aeberhard

Received: date / Accepted: date

**Abstract** Si-SiO<sub>x</sub> superlattices are among the candidates that have been proposed as high band gap absorber material in all-Si tandem solar cell devices. Due to the large potential barriers for photoexcited charge carriers, transport in these devices is restricted to quantum confined superlattice states. As a consequence of the finite number of wells, large built-in fields and any kind of disorder, the electronic spectrum can deviate considerably from the minibands of a regular superlattice. In this paper, a quantum-kinetic theory based on the non-equilibrium Green's function formalism for an effective mass Hamiltonian is used to investigate photogeneration and transport in such devices for arbitrary geometry and operating conditions. By including the coupling of electrons to both photons and phonons, the theory is able to provide a microscopic picture of indirect generation, carrier relaxation and inter-well transport mechanisms beyond the ballistic regime.

**Keywords** solar cell · superlattice · quantum transport · NEGF

## 1 Introduction

Si-SiO<sub>x</sub> superlattices have been proposed as candidates for the high band gap absorber component in all-Si tandem solar cells [1, 2]. In these devices, photocurrent flow is enabled via the overlap of states in neighboring Si quantum wells separated by ultra-thin oxide layers, i.e. unlike in the case of an intermediate band solar cell,

the superlattice states contribute to the optical transitions and at the same time provide transport of photo-carriers, which makes it necessary to control both the optical and the transport properties of the multilayer structure. To this end, a suitable theoretical picture of the optoelectronic processes in such type of structures is highly desirable.

There are several peculiar aspects of the device which require special consideration in the choice of an appropriate model. First of all, a microscopic model for the electronic structure is indispensable, since the relevant states are those of an array of strongly coupled quantum wells. In a standard approach, these states are described with simple Kronig-Penney models for a regular, infinitely extended superlattice. The superlattice dispersion obtained in this way can then be used to determine an effective density of states as well as the absorption coefficient to be used in macroscopic 1D solar cell device simulators. However, depending on the internal field and the structural disorder, the heterostructure states may deviate considerably from regular minibands or can even form Wannier-Stark ladders. Furthermore, the charge carrier mobility, which has a crucial impact on the charge collection efficiency in solar cells, depends on the dominant transport regime at given operating conditions, which may be described by miniband transport, sequential tunneling or Wannier-Stark hopping [3], relying on processes that are not accessible to standard macroscopic transport models.

In this paper, the photovoltaic properties of quantum well superlattice absorbers are investigated numerically on the example of a Si-SiO<sub>x</sub> multilayer structure embedded in the intrinsic region of a *p-i-n* diode, using a multiband effective mass approximation for the electronic structure and the non-equilibrium Green's function (NEGF) formalism for inelastic quantum trans-

---

U. Aeberhard  
IEF-5: Photovoltaik, Forschungszentrum Jülich, D-52425 Jülich, Germany  
Tel: +49 2461 61 2615  
E-mail: u.aeberhard@fz-juelich.de

port, which permits to treat on equal footing both coherent and incoherent transport as well as phonon-assisted optical transitions at arbitrary internal fields and heterostructure potentials.

## 2 Theoretical Model

In order to enable a sound theoretical description of the pivotal photovoltaic processes in semiconductor nanostructures, i.e. charge carrier generation, recombination and collection, both optical transitions and inelastic quantum transport are to be treated on equal footing within a consistent microscopic model. To this end, a theoretical framework based on the NEGF formalism was developed [4,5] and applied to quantum well solar cell devices. Here, we reformulate the theory for a multiband effective mass Hamiltonian, similar to [6, 7], and extend it to cover the phonon-assisted indirect transitions that dominate the photovoltaic processes in Si-based devices. Furthermore, in difference to the former case, both photogeneration and transport processes take place within superlattice states, since escape of carriers to continuum states is not possible due to the large band offsets.

### 2.1 Hamiltonian and basis

The full quantum photovoltaic device is described in terms of the model Hamiltonian

$$\hat{H} = \hat{H}_e + \hat{H}_\gamma + \hat{H}_p, \quad (\text{total}) \quad (1)$$

$$\hat{H}_e = \hat{H}_e^0 + \hat{H}_e^i, \quad (\text{electronic}) \quad (2)$$

$$\hat{H}_e^i = \hat{H}_{e\gamma} + \hat{H}_{ep} + \hat{H}_{ee}, \quad (\text{interaction}) \quad (3)$$

consisting of the coupled systems of electrons ( $\hat{H}_e$ ), photons ( $\hat{H}_\gamma$ ) and phonons ( $\hat{H}_p$ ). Since the focus is on the electronic device characteristics, only  $\hat{H}_e$  is considered here, however including all of the terms corresponding to coupling to the bosonic systems.

The electronic system without coupling to the bosonic degrees of freedom is described by

$$\hat{H}_e^0 = -\frac{\hbar^2}{2m_0}\Delta + \tilde{U}(z), \quad (4)$$

with

$$\tilde{U}(z) = U(z) + V_0(z), \quad (5)$$

where  $V_0$  is the heterostructure potential and  $U$  is the Hartree term of the Coulomb interaction corresponding to the solution of Poisson's equation that considers carrier-carrier interactions ( $\hat{H}_{ee}$ ) on a mean-field level.

The Hamiltonian representations for the interaction terms are obtained starting from the single particle interaction potentials. For the electron-photon interaction, the latter is given via the linear coupling to the vector potential operator of the electromagnetic field  $\hat{\mathbf{A}}$ ,

$$\hat{H}_{e\gamma} = -\frac{e}{m_0}\hat{\mathbf{A}} \cdot \hat{\mathbf{p}} \quad (6)$$

with  $\hat{\mathbf{p}}$  the momentum operator and

$$\hat{\mathbf{A}}(\mathbf{r}, t) = \sum_{\lambda, \mathbf{q}} \left[ \mathbf{A}_0(\lambda, \mathbf{q})\hat{b}_{\lambda, \mathbf{q}}(t) + \mathbf{A}_0^*(\lambda, -\mathbf{q})\hat{b}_{\lambda, -\mathbf{q}}^\dagger(t) \right] \times e^{i\mathbf{q}\mathbf{r}}, \quad (7)$$

$$\mathbf{A}_0(\lambda, \mathbf{q}) = \frac{\hbar}{\sqrt{2\epsilon_0 V \hbar \omega_{\mathbf{q}}}} \epsilon_{\lambda \mathbf{q}}, \quad (8)$$

where  $\epsilon_{\lambda \mathbf{q}}$  is the polarization of the photon with wave vector  $\mathbf{q}$  and energy  $\hbar \omega_{\mathbf{q}}$  added to or removed from photon mode  $(\lambda, \mathbf{q})$  by the bosonic creation and annihilation operators

$$\hat{b}_{\lambda, \mathbf{q}}^\dagger(t) = \hat{b}_{\lambda, \mathbf{q}}^\dagger e^{i\omega_{\mathbf{q}}t}, \quad \hat{b}_{\lambda, \mathbf{q}}(t) = \hat{b}_{\lambda, \mathbf{q}} e^{-i\omega_{\mathbf{q}}t}, \quad (9)$$

and  $V$  is the absorbing volume.

The vibrational degrees of freedom of the system are described in terms of the coupling of the force field of the electron-ion potential  $V_{ei}$  to the quantized field  $\hat{\mathbf{U}}$  of the ionic displacement [8],

$$\hat{H}_{ep}(\mathbf{r}, t) = \sum_{\mathbf{L}, \boldsymbol{\kappa}} \hat{\mathbf{U}}(\mathbf{L} + \boldsymbol{\kappa}, t) \cdot \nabla V_{ei}[\mathbf{r} - (\mathbf{L} + \boldsymbol{\kappa})], \quad (10)$$

with the displacement field given by the Fourier expansion

$$\hat{\mathbf{U}}_\alpha(\mathbf{L}\boldsymbol{\kappa}, t) = \sum_{\Lambda, \mathbf{Q}} \mathcal{U}_{\alpha\boldsymbol{\kappa}}(\Lambda, \mathbf{Q}) e^{i\mathbf{Q} \cdot (\mathbf{L} + \boldsymbol{\kappa})} [\hat{a}_{\Lambda, \mathbf{Q}}(t) + \hat{a}_{\Lambda, -\mathbf{Q}}^\dagger(t)], \quad (11)$$

where the ion equilibrium position is  $\mathbf{L} + \boldsymbol{\kappa}$ , with  $\mathbf{L}$  the lattice position and  $\boldsymbol{\kappa}$  the relative position of a specific basis atom at this lattice site, and  $\hat{a}_{\Lambda, \mathbf{Q}}, \hat{a}_{\Lambda, \mathbf{Q}}^\dagger$  are the bosonic creation and annihilation operators for a (bulk) phonon mode with polarization  $\Lambda$  and wave vector  $\mathbf{Q}$  in the first Brillouin zone. The corresponding polarization vector is  $\epsilon_{\alpha\boldsymbol{\kappa}\Lambda}(\mathbf{Q})$ .

For numerical implementation of the model, the above Hamiltonian needs to be represented in a suitable basis. Due to the amorphous nature of the  $\text{SiO}_x$  layers, atomistic models are of limited applicability. Furthermore, the use of an effective mass theory simplifies the electronic model considerably. For a quasi-one-dimensional multilayer system, where quantization appears only in

the vertical (growth) direction, the corresponding basis functions have the form

$$\psi_{i\mathbf{k}_{\parallel}}(\mathbf{r}) = \varphi_{i\mathbf{k}_{\parallel}}(\mathbf{r})u_{n\mathbf{k}_0}(\mathbf{r}), \quad (12)$$

where  $\varphi_{i\mathbf{k}_{\parallel}}$  is the envelope basis function for discrete spatial (layer) index  $i$  (longitudinal) and transverse momentum  $\mathbf{k}_{\parallel}$ ,  $u_{n\mathbf{k}_0}$  is the Bloch function of bulk band  $n$ , centered on  $\mathbf{k}_0$ . In the case of a system with large transverse extension, the envelope basis function can be written as

$$\varphi_{i\mathbf{k}_{\parallel}}(\mathbf{r}) = \frac{e^{i\mathbf{k}_{\parallel}\mathbf{r}_{\parallel}}}{\sqrt{S}}\chi_i(z), \quad (13)$$

where  $\mathbf{r}_{\parallel} = (x, y)$ ,  $S$  is the cross sectional area and  $\chi_i$  is the localized longitudinal envelope function basis element. For the latter, finite element shape functions are a popular choice [7, 9]. Here, we will use a simple finite difference basis equivalent to a separate single band tight-binding approach for each band [10, 11, 12]. In the above basis, the fermion field operators for the charge carriers are represented via

$$\hat{\Psi}(\mathbf{r}, t) = \sum_{i, n, \mathbf{k}_{\parallel}} \psi_{i\mathbf{k}_{\parallel}}(\mathbf{r})\hat{c}_{i\mathbf{k}_{\parallel}}(t), \quad (14)$$

$$\hat{\Psi}^{\dagger}(\mathbf{r}, t) = \sum_{i, n, \mathbf{k}_{\parallel}} \psi_{i\mathbf{k}_{\parallel}}^*(\mathbf{r})\hat{c}_{i\mathbf{k}_{\parallel}}^{\dagger}(t), \quad (15)$$

where  $\hat{c}^{\dagger}, \hat{c}$  are single fermion creation and annihilation operators. The representation of the model system Hamiltonian in the above basis is now obtained in standard second quantization, i.e.

$$\mathcal{H}(t) = \int d^3r \hat{\Psi}^{\dagger}(\mathbf{r}, t)\hat{H}_e^0\hat{\Psi}(\mathbf{r}, t) \quad (16)$$

$$= \sum_{i, j} \sum_{n, m} \sum_{\mathbf{k}_{\parallel}} H_{in; jm}(\mathbf{k}_{\parallel})\hat{c}_{i\mathbf{k}_{\parallel}}^{\dagger}(t)\hat{c}_{j\mathbf{k}_{\parallel}}(t). \quad (17)$$

## 2.2 Green's functions, self energies and quantum kinetic equations

Within the non-equilibrium Green's function theory of quantum optics and transport in excited semiconductor nanostructures, physical quantities are expressed in terms of quantum statistical ensemble averages of single particle operators for the interacting quasiparticles introduced above, namely the fermion field operator  $\hat{\Psi}$  for the charge carriers, the quantized photon field vector potential  $\hat{\mathbf{A}}$  for the photons and the ionic displacement field  $\hat{\mathbf{U}}$  for the phonons. The corresponding

Green's functions are

$$\mathcal{G}(\underline{1}, \underline{2}) = -\frac{i}{\hbar}\langle\hat{\Psi}(\underline{1})\hat{\Psi}^{\dagger}(\underline{2})\rangle_C, \quad (\text{electrons}) \quad (18)$$

$$\mathcal{D}_{ik}^{\gamma}(\underline{1}, \underline{2}) = -\frac{i}{\hbar}\langle\hat{A}_i(\underline{1})\hat{A}_k(\underline{2})\rangle_C, \quad (\text{photons}) \quad (19)$$

$$\mathcal{D}_{\alpha\beta}^p(\underline{1}, \underline{2}) = -\frac{i}{\hbar}\langle\hat{U}_{\alpha}(\underline{1})\hat{U}_{\beta}(\underline{2})\rangle_C, \quad (\text{phonons}) \quad (20)$$

where  $\langle\dots\rangle_C$  denotes the contour ordered operator average peculiar to non-equilibrium quantum statistical mechanics [13, 14] for arguments  $\underline{1} = (\mathbf{r}_1, t_1)$  with temporal components on the Keldysh contour [14].

The Green's functions follow as the solutions to corresponding *Dyson's equations* [15, 16, 17, 8],

$$\begin{aligned} \int d\mathfrak{z} [\mathcal{G}_0^{-1}(\underline{1}, \mathfrak{z}) - \Sigma(\underline{1}, \mathfrak{z})] \mathcal{G}(\mathfrak{z}, \underline{2}) &= \delta(\underline{1} - \underline{2}), \\ \int d\mathfrak{z} [(\overleftrightarrow{\mathcal{D}}_0^{\gamma})^{-1}(\underline{1}, \mathfrak{z}) - \overleftrightarrow{\mathbf{H}}^{\gamma}(\underline{1}, \mathfrak{z})] \overleftrightarrow{\mathcal{D}}^{\gamma}(\mathfrak{z}, \underline{2}) &= \overleftrightarrow{\delta}(\underline{1} - \underline{2}), \\ \int d\mathfrak{z} [(\mathcal{D}_0^p)^{-1}(\underline{1}, \mathfrak{z}) - \mathbf{P}^p(\underline{1}, \mathfrak{z})] \mathcal{D}^p(\mathfrak{z}, \underline{2}) &= \delta(\underline{1} - \underline{2}). \end{aligned} \quad (21)$$

$\mathcal{G}_0$ ,  $\mathcal{D}_0^{\gamma}$  and  $\mathcal{D}_0^p$  are the propagators for noninteracting electrons, photons and phonons, respectively,  $\leftrightarrow$  denotes transverse and boldface tensorial quantities. The electronic self-energy  $\Sigma$  encodes the renormalization of the charge carrier Green's functions due to the interactions with photons and phonons, i.e. generation, recombination and relaxation processes. Charge injection and absorption at contacts is considered via an additional boundary self-energy term reflecting the openness of the system. The photon and phonon self-energy tensors  $\overleftrightarrow{\mathbf{H}}^{\gamma}$  and  $\mathbf{P}^p$  describe the renormalization of the optical and vibrational modes, leading to phenomena such as photon recycling or the phonon bottleneck responsible for hot carrier effects. The self-energies can be derived either via perturbative methods using a diagrammatic approach or a Wick factorization or using variational derivatives. In the following, any renormalizing effect of the electronic system on the photons and phonons is neglected, i.e. the coupling to the bosons corresponds to the connection to corresponding equilibrium reservoirs. While this treatment is generally a good approximation in the case of phonons, it is valid for the coupling to the photonic systems only in the case of low absorption, i.e. weak coupling or very short absorber length.

The use of the equilibrium boson propagators implies that only the electronic Dyson equations are solved. In the chosen discrete real-space basis, the components of the steady-state Dyson and Keldysh equations for electronic Greens functions are turned into a linear sys-

$\text{tem}^1(\nu = \mathbf{k}_{\parallel}, E)$

$$\mathbf{G}^R(\nu) = \left[ \{ \mathbf{G}_0^R(\nu) \}^{-1} - \Sigma^{RI}(\nu) - \Sigma^{RB}(\nu) \right]^{-1}, \quad (22)$$

$$\mathbf{G}_0^R(\nu) = [(E + i\eta)\mathbb{1} - \mathbf{h}(\mathbf{k}_{\parallel})]^{-1}, \quad (23)$$

$$\mathbf{G}^A(\nu) = [\mathbf{G}^R(\nu)]^\dagger, \quad (24)$$

$$\mathbf{G}^{\lessgtr}(\nu) = \mathbf{G}^R(\nu) \left[ \Sigma^{\lessgtr I}(\nu) + \Sigma^{\lessgtr B}(\nu) \right] \mathbf{G}^A(\nu), \quad (25)$$

for each total energy  $E$  and transverse momentum  $\mathbf{k}_{\parallel}$ . There are two types of self-energies in the above equations. The term  $\Sigma^I$  is due to the interactions between the different degrees of freedom of the system. The expressions for electron-photon and electron-phonon interaction are determined as the Fock term within many-body perturbation theory on the level of a selfconsistent Born approximation, and using the equilibrium boson propagators, they are obtained in the following form, ( $\alpha = \gamma, p$ )

$$\begin{aligned} \Sigma_{e\alpha}^{\lessgtr}(\mathbf{k}_{\parallel}; E) &= \sum_{\lambda, \mathbf{q}} \mathcal{M}^{e\alpha}(\mathbf{k}_{\parallel}, \mathbf{q}, \lambda) [N_{\lambda, \mathbf{q}}^{\alpha} \mathbf{G}^{\lessgtr}(\mathbf{k}_{\parallel}; E \mp \hbar\omega_{\lambda, \mathbf{q}}) \\ &\quad + (N_{\lambda, \mathbf{q}}^{\alpha} + 1) \mathbf{G}^{\lessgtr}(\mathbf{k}_{\parallel}; E \pm \hbar\omega_{\lambda, \mathbf{q}})] \\ &\quad \times \mathcal{M}^{e\alpha}(\mathbf{k}_{\parallel}, -\mathbf{q}, \lambda) \end{aligned} \quad (26)$$

and

$$\begin{aligned} \Sigma_{e\alpha}^{R,A}(\mathbf{k}_{\parallel}; E) &= i \int \frac{dE'}{2\pi} \frac{\Sigma_{e\alpha}^>(\mathbf{k}_{\parallel}; E') - \Sigma_{e\alpha}^<(\mathbf{k}_{\parallel}; E')}{E' - E \pm i\eta} \\ &= \mathcal{P} \int \frac{dE'}{2\pi} \frac{\Gamma(\mathbf{k}_{\parallel}; E')}{E' - E} \mp \frac{i}{2} \Gamma(\mathbf{k}_{\parallel}; E), \end{aligned} \quad (27)$$

where

$$\Gamma(\mathbf{k}_{\parallel}; E) = i [\Sigma_{e\alpha}^>(\mathbf{k}_{\parallel}; E) - \Sigma_{e\alpha}^<(\mathbf{k}_{\parallel}; E)]. \quad (28)$$

Since the principal value integral corresponds to the real part of the self energy and thus to the renormalization of the electronic structure, which is both small and irrelevant for the photovoltaic performance, it is neglected in the numerical implementation.

Once the Green's functions and self-energies have been determined via self-consistent solution of Eqs. (22)-(25) and (26)-(27), they can be directly used to express the physical quantities that characterize the system, such as charge carrier and current densities as well as the rates for the different scattering processes.

<sup>1</sup> In steady-state, the Green's functions depend only on the difference  $\tau = t - t'$  of the real-time variables, which is Fourier-transformed to energy.

### 2.3 Microscopic optoelectronic conservation laws and scattering rates

The macroscopic balance equation for a photovoltaic system is the steady state continuity equation for the charge carrier density

$$\nabla \cdot \mathbf{j}_c(\mathbf{r}) = \mathcal{G}_c(\mathbf{r}) - \mathcal{R}_c(\mathbf{r}), \quad c = e, h, \quad (29)$$

where  $j_c$  is the particle current density,  $\mathcal{G}_c$  the generation rate and  $\mathcal{R}_c$  the recombination rate of carriers species  $c^2$ . In the microscopic theory, the divergence of the electron (particle) current is given by [13, 14]

$$\begin{aligned} \nabla \cdot \mathbf{j}(\mathbf{r}) &= -\frac{2}{V} \int \frac{dE}{2\pi\hbar} \int d^3r' \left[ \Sigma^R(\mathbf{r}, \mathbf{r}'; E) G^<(\mathbf{r}', \mathbf{r}; E) \right. \\ &\quad \left. + \Sigma^<(\mathbf{r}, \mathbf{r}'; E) G^A(\mathbf{r}', \mathbf{r}; E) - G^R(\mathbf{r}, \mathbf{r}'; E) \right. \\ &\quad \left. \times \Sigma^<(\mathbf{r}', \mathbf{r}; E) - G^<(\mathbf{r}, \mathbf{r}'; E) \Sigma^A(\mathbf{r}', \mathbf{r}; E) \right]. \end{aligned} \quad (30)$$

If the integration is restricted to either conduction or valence bands, the above equation corresponds to the microscopic version of (29) and provides on the RHS the total *local* interband scattering rate. The total interband current is found by integrating the divergence over the absorbing/emitting volume, and is equivalent to the total *global* transition rate and, via the Gauss theorem, to the difference of the interband currents at the boundaries of the interacting region. Making use of the cyclic property of the trace, it can be expressed in the form

$$\begin{aligned} R &= \frac{2}{V} \int d^3r \int \frac{dE}{2\pi\hbar} \int d^3r' \left[ \Sigma^<(\mathbf{r}, \mathbf{r}'; E) G^>(\mathbf{r}', \mathbf{r}; E) \right. \\ &\quad \left. - \Sigma^>(\mathbf{r}, \mathbf{r}'; E) G^<(\mathbf{r}', \mathbf{r}; E) \right], \end{aligned} \quad (31)$$

with units  $[R] = s^{-1}$ . If we are interested in the interband scattering rate, we can neglect in Eq. (31) the contributions to the self-energy from *intra*band scattering, e.g. via interaction with phonons, low energy photons (free carrier absorption) or ionized impurities, since they cancel upon energy integration over the band. Since inequivalent conduction band valleys may be described by different bands, the corresponding inter-valley scattering process has also interband character with a nonvanishing rate, as long as only one of the valleys is considered in the rate evaluation. Furthermore, if self-energies and Green's functions are determined self-consistently as they must in order to guarantee current conservation, the Green's functions are related to the scattering self-energies via the Dyson equation for the propagator and the Keldysh equation for the correlation functions as given in Eqs. (22)-(25), and will thus be

<sup>2</sup> The dimensions are that of a volume rate,  $[\mathcal{G}, \mathcal{R}] = m^{-3}s^{-1}$ .

modified due to the intraband scattering. In the present case of indirect optical transitions, the Greens functions entering the rate for electron-photon scattering between the  $\Gamma$  bands are the solutions of Dyson equations with an intervalley phonon scattering self-energy and may thus contain contributions from the  $X$ -valleys. In the same way, the  $\Gamma_c$  Greens functions entering the electron-phonon  $\Gamma_c - X$  scattering rate contain a photo-generated contribution. By this way, indirect, phonon-assisted optical transitions are enabled.

### 3 Implementation for Si-SiO<sub>x</sub> superlattice absorbers

#### 3.1 Electronic structure model

Within the EMA for silicon chosen for this work, the electrons are described by a multi-valley picture with different values for transverse and longitudinal effective mass, similar to [18]. However, for simplicity, in the case of transverse  $X$  valleys ( $X_{\parallel}$ ), the anisotropy in the transverse mass is neglected and an average value is used. The virtual  $\Gamma$  states used in the indirect transitions are described by an additional (negative) mass. The holes are modelled by two decoupled single bands with different effective masses corresponding to heavy and light holes. Thus, in total, five bands are used to describe the electronic structure, three for the electrons ( $X_{\parallel}$ ,  $X_{\perp}$ ,  $\Gamma_c$ ) and two for the holes ( $\Gamma_{vl}$ ,  $\Gamma_{vh}$ ). The band parameters used in the simulations are listed in Tab. 1. For each band, a set of Green's functions are computed from the corresponding decoupled Dyson and Keldysh equations. In the computation of physical quantities such as electron and hole densities as well as the corresponding current densities, the summation over all conduction or valence bands needs to be performed,

$$n_i = \sum_{b=\Gamma_c, X_{\parallel}, X_{\perp}} f_b n_{i,b} \quad (32)$$

$$= \sum_b f_b \sum_{\mathbf{k}_{\parallel}} \int \frac{dE}{\pi A \Delta} (-i) G_{ii,b}^<(\mathbf{k}_{\parallel}; E), \quad (33)$$

where  $f_b$  denotes the degeneracy of the conduction bands, which is  $f_{\Gamma_c} = 1$ ,  $f_{X_{\parallel}} = 4$  and  $f_{X_{\perp}} = 2$ . Similarly, the electron current in terms of the Green's functions reads

$$J_i = \sum_{b=\Gamma_c, X_{\parallel}, X_{\perp}} f_b J_{i,b} \quad (34)$$

$$= \sum_b f_b \sum_{\mathbf{k}_{\parallel}} \int \frac{dE}{\pi \hbar A} [t_{i+1} G_{i+1,i,b}^<(\mathbf{k}_{\parallel}; E) - t_{i+1} G_{ii+1,b}^<(\mathbf{k}_{\parallel}; E)]. \quad (35)$$

For the chosen model of the bulk band structure, the total radiative rate is

$$R_{e\gamma} = \frac{2}{\hbar \mathcal{A}} \int_{\Gamma_c} \frac{dE}{2\pi} \text{Tr} \left\{ \sum_{\mathbf{k}_{\parallel}} [\Sigma_{e\gamma, \Gamma_c}^>(\mathbf{k}_{\parallel}; E) \mathbf{G}_{\Gamma_c}^<(\mathbf{k}_{\parallel}; E) - \Sigma_{e\gamma, \Gamma_c}^<(\mathbf{k}_{\parallel}; E) \mathbf{G}_{\Gamma_c}^>(\mathbf{k}_{\parallel}; E)] \right\}, \quad (36)$$

and the inter-valley phonon scattering rate reads

$$R_{ep, \Gamma-X} = \frac{2}{\hbar \mathcal{A}} \int_{\Gamma_c} \frac{dE}{2\pi} \text{Tr} \left\{ \sum_{\mathbf{k}_{\parallel}} [\Sigma_{ep(\Gamma-X), \Gamma_c}^>(\mathbf{k}_{\parallel}; E) \times \mathbf{G}_{\Gamma_c}^<(\mathbf{k}_{\parallel}; E) - \Sigma_{ep(\Gamma-X), \Gamma_c}^<(\mathbf{k}_{\parallel}; E) \mathbf{G}_{\Gamma_c}^>(\mathbf{k}_{\parallel}; E)] \right\}. \quad (37)$$

#### 3.2 Interaction parameters

Optical transitions are assumed to take place only at the center of the Brillouin zone, i.e. between  $\Gamma_v$  and virtual  $\Gamma_c$  states, the latter being (de-)populated via phonon scattering from (to) the  $X$  valleys, which carry the photocurrent. All other transition channels, e.g. phonon scattering in the valence band prior to photon absorption, are neglected at this stage. The momentum matrix element in the electron-photon coupling is thus to be taken between the  $\Gamma_v$  and  $\Gamma_c$  bands at  $\mathbf{k}_0 = \mathbf{0}$ . The interaction matrix elements are evaluated using an average effective coupling for both light and heavy holes.

Four different types of phonons are used in the present work to describe both carrier relaxation as well as phonon assisted optical transitions. For the relaxation process,  $X - X$  inter-valley scattering is used for the electrons and non-polar optical phonon scattering for the holes. Further broadening is added for both carrier species through acoustic phonon scattering in the deformation potential formulation. Finally, the momentum transfer for the indirect optical transitions is mediated via  $\Gamma_c - X$  intervalley scattering.

**Table 1** Band parameters used in simulations

	Si	SiO <sub>x</sub>
$m_{\Gamma_c}^*/m_0$	-0.3	-0.3
$m_{X_{\parallel}}^*/m_0$	0.98	0.4
$m_{X_{\perp}}^*/m_0$	0.19	0.4
$m_{\Gamma_v, lh}^*/m_0$	0.16	0.4
$m_{\Gamma_v, hh}^*/m_0$	0.49	0.4
$E_{g, \Gamma_v - \Gamma_c}$ [eV]	3.5	5.5
$E_{g, \Gamma_v - X}$ [eV]	1.1	3.1

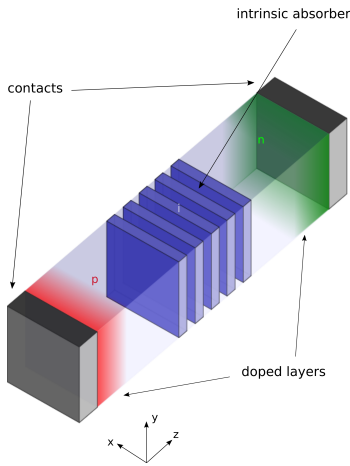


**Fig. 1** Spatial structure of the  $p$ - $i(SL)$ - $n$  model system.

## 4 Numerical results and discussion

### 4.1 Model system

The model system under investigation is shown schematically in Fig. 1. It consists of a set of four coupled quantum wells of 6 monolayer (ML) width with layers separated by oxide barriers of 3 ML thickness, embedded in the intrinsic region of a Si  $p$ - $i$ - $n$  diode. The thickness of the doped layers is 50 ML, while the total length of the  $i$ -region amounts to 154 ML. This composition and doping leads to the band diagram shown in Fig. 2.

### 4.2 Density of states

Insertion of the oxide barriers leads to an increase of the effective band gap in the central region of the diode from 1.1 eV to  $\sim 1.3$  eV, as seen in Fig. 3, which shows

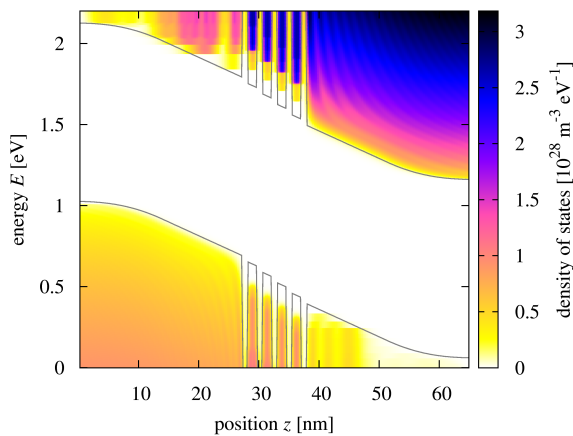


**Fig. 3** Transverse momentum integrated local density of states of the  $p$ - $i(SL)$ - $n$  photodiode at short circuit conditions.

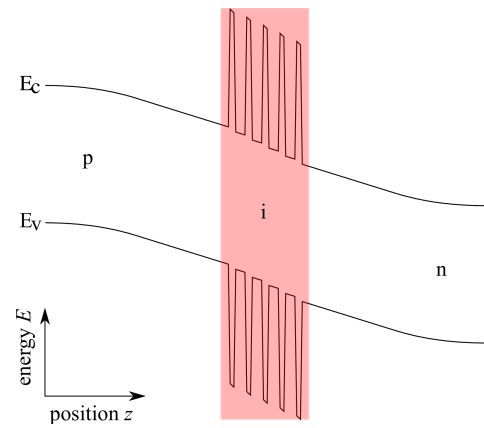


**Fig. 2** Band diagram of the  $p$ - $i(SL)$ - $n$  model system.

the transverse momentum integrated local density of states. In the actual situation of strong band bending, quantization also occurs in the form of notch states in front of the barriers. The density of states at minority carrier contacts is additionally depleted due to the imposition of closed system boundary conditions that prevents the formation of a dark leakage current under bias. The density of states component at zero transverse momentum displayed in Fig. 4 allows the identification of the confined states in the different quantum wells, which are considerably localized due to the large internal field, with however finite overlap between neighboring wells in the case of the higher states. The ground state is split due to the different effective masses of the charge carriers, the effect being more pronounced for the electrons.

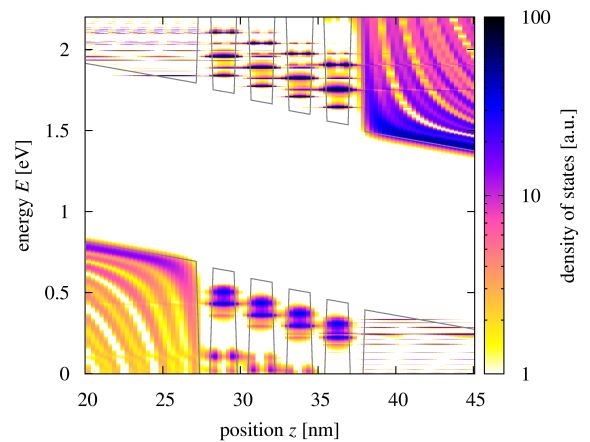


**Fig. 4** Local density of states in the quantum well region at zero transverse momentum ( $k_{\parallel} = 0$ ).

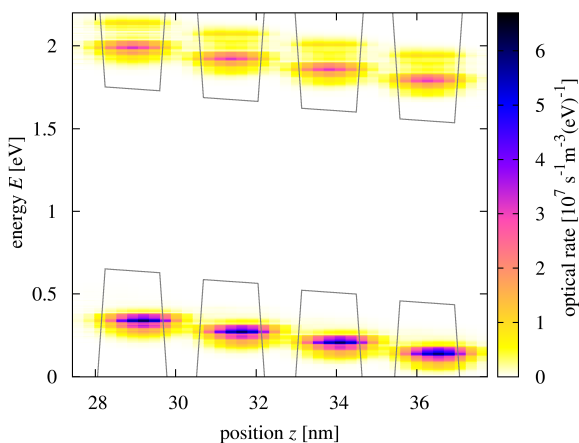


**Fig. 5** Spatially and energy resolved photon carrier photogeneration rate in the quantum well region at short circuit conditions and under monochromatic illumination with energy  $E_\gamma = 1.65$  eV and intensity  $I_\gamma = 10$  kW/m<sup>2</sup>.

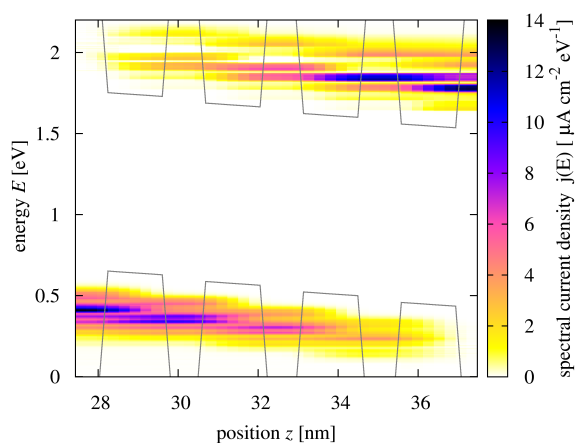


**Fig. 6** Spatially and energy resolved photon carrier short-circuit photocurrent density in the quantum well region under monochromatic illumination with energy  $E_\gamma = 1.65$  eV and intensity  $I_\gamma = 10$  kW/m<sup>2</sup>.

### 4.3 Generation and photocurrent spectrum

The spectral rate of carrier generation in the confined states under illumination with monochromatic light at photon energy  $E_\gamma = 1.65$  eV and intensity  $I_\gamma = 10$  kW/m<sup>2</sup> is shown in Fig. 5. At this photon energy, both lowest and second minibands are populated. The photocurrent originating in this excitation is shown in Fig. 6. Current flows also in both first and second minibands, i.e. over the whole spectral range of generation, which means that relaxation due to scattering is not fast enough to confine transport to the band edge. However, transport of photocarriers is strongly affected by the inelastic interactions and is closest to the sequential tunneling regime.

## 5 Conclusions

In this paper, an adequate theoretical description of photogeneration and transport in Si-SiO<sub>x</sub> superlattice absorbers was presented. Based on quantum kinetic theory, the formalism allows a unified approach to both quantum optics and inelastic quantum transport and is thus able to capture pivotal features of photogeneration and photocarrier extraction in Si-based coupled quantum well structures, such as phonon-assisted optical transitions and field-dependent transport in superlattice states. Due to the microscopic nature of the theory, energy resolved information can be obtained, such as the spectra for photogeneration rate and photocurrent density, which shows that in the case of high internal fields, excess charge is transported via sequential tunneling in the miniband where it is generated.

## Acknowledgements

Financial support was provided by the German Federal Ministry of Education and Research (BMBF) under Grant No. 03SF0352E.

## References

1. M.A. Green, *Materials Science and Engineering B* **74**(1-3), 118 (2000)
2. M.A. Green, *Prog. Photovolt: Res. Appl.* **9**, 123 (2001)
3. A. Wacker, *Phys. Rep.* **357**, 1 (2002)
4. U. Aeberhard, R. Morf, *Phys. Rev. B* **77**, 125343 (2008)
5. U. Aeberhard, *A Microscopic Theory of Quantum Well Photovoltaics*. Ph.D. thesis, ETH Zuerich (2008)
6. S. Steiger, R. Veprek, B. Witzigmann, in *Proc. IWCE* (2009)
7. S. Steiger, *Modeling Nano-LED*. Ph.D. thesis, ETH Zuerich (2009)
8. W. Schäfer, M. Wegener, *Semiconductor Optics and Transport Phenomena* (Springer, 2002)
9. T. Kubis, C. Yeh, P. Vogl, A. Benz, G. Fasching, C. Deutsch, *Phys. Rev. B* **79**, 195323 (2009)
10. R. Lake, G. Klimeck, R. Bowen, D. Jovanovic, *J. Appl. Phys.* **81**, 7845 (1997)
11. L.E. Henrickson, *J. Appl. Phys.* **91**, 6273 (2002)
12. S. Jin, *Modeling of Quantum Transport in Nano-Scale MOSFET Devices*. Ph.D. thesis, School of Electrical Engineering and Computer Science College of Engineering, Seoul National University (2006)
13. L.P. Kadanoff, G. Baym, *Quantum Statistical Mechanics* (Benjamin, Reading, Mass., 1962)
14. L. Keldysh, *Sov. Phys.-JETP*. **20**, 1018 (1965)
15. K. Henneberger, H. Haug, *Phys. Rev. B* **38**, 9759 (1988)
16. M. Pereira, K. Henneberger, *Phys. Rev. B* **53**, 16485 (1996)
17. M. Pereira, K. Henneberger, *Phys. Rev. B* **58**, 2064 (1998)
18. S. Jin, Y.J. Park, H.S. Min, *J. Appl. Phys.* **99**, 123719 (2006)